WSG

WSG-RR 8/96

The Integration of Remote Sensing and Ancillary Data

Florian Kressler

Institut für Wirtschafts-
und Sozialgeographie

**Wirtschaftsuniversität
Wien**

Department of Economic
and Social Geography

**Vienna University of
Economics and Business
Administration**

WSG-RR 8/96

The Integration of Remote Sensing

and Ancillary Data

Florian Kressler

WSG-RR 8/96

The Integration of Remote Sensing and Ancillary Data

Florian Kressler

WSG-Research Report 8

March 1996

Foreword

This thesis was written at the University of Economics and Business Administration, Department of Geography, in co-operation with the Austrian Research Center, Seibersdorf, Department for Environmental Planning. It was supported by a scholarship granted by the Austrian Research Center, Seibersdorf, who also provided the necessary technical facilities. A study year at the University of California, Santa Barbara, USA with the Education Abroad Program gave me the opportunity to learn in-depth about remote sensing and the analysis of satellite images which led to the opportunity of writing this thesis.

I would like to thank Professor Manfred Fischer for his suggestions during the writing of this thesis and for the final evaluation, Dr. Klaus Steinnocher, Austrian Research Center, Seibersdorf, for initiating this thesis and his supportive collaboration, Mag. Petra Staufer for her parts of the evaluation process, proof-reading, and helpful suggestions, and DI. Wilmersdorfer of MD-ADV, City of Vienna, for making the land-use data available. I also would like to thank my parents for providing the basis for my academic studies and for supporting decisions, even if an immediate benefit could not always be clearly seen.

Table of Contents

List of Figures

List of Tables

Abstract

Obtaining up-to-date information concerning the environment at reasonable costs is a challenge faced by many institutions today. Satellite images meet both demands and thus present a very attractive source of information.

The following thesis deals with the comparison of satellite images and a vector based land use data base of the City of Vienna. The satellite data is transformed using the spectral mixture analysis, which allows an investigation at a sub-pixel level. The results of the transformation are used to determine how suitable this spectral mixture analysis is to distinguish different land use classes in an urban area. In a next step the results of the spectral mixture analysis of two different images (recorded in 1986 and 1991) are used to undertake a change detection. The aim is to show those areas, where building activities have taken place. This information may aid the update of data bases, by limiting a detailed examination of an area to those areas, which show up as changes in the change detection.

The proposed method is a fast and inexpensive way of analysing large areas and highlighting those areas where changes have taken place. It is not limited to urban areas but may easily be adapted for different environments.

Key Words: Remote Sensing, Spectral Mixture Analysis, Urban, Change Detection, Landsat

1. Introduction

Since the launch of Landsat 1 in 1972 satellite remote sensing has become an integral part in the monitoring of the earth's environment. For the first time it is possible to receive satellite images on a regular basis from most parts of the world at relatively low costs. Despite the initial disappointment due to the low spatial resolution (79 x 79 m²) of the recording devices (Multispectral Scanner) satellite images have been used successfully for many different applications, e.g. forest inventory, crop type discrimination, and so forth (Avery and Berlin, 1992). Landsats 4 and 5 feature an improved scanning device (Thematic Mapper) with higher spatial (30 x 30 m²) and spectral resolution. This makes a much more detailed analysis of the environment possible. As satellite sensors are being developed with even better spatial and spectral resolutions new applications will be possible and existing ones made easier. While these sensors are still under development or in the experimental stage, different methods, which might be used on the data collected by the new sensors, must be examined now.

The aforementioned improved resolutions also mean an exponential increase of data volume. This poses new challenges for the analysis of satellite images and even though computers are becoming more and more powerful, efficient and fast routines must be found to extract the desired information.

A successful integration of remote sensing and ancillary data is important to use the advantages of both data concepts. Data from satellites offer the advantages of being up to date and relatively inexpensive whereas the ancillary data (e.g. database concerning a certain area) offer a higher information level. The aim of this thesis is to show how satellite data may be used to facilitate the update of urban land use databases. Satellite images of urban areas, as compared to a natural environment, add the challenge of being very heterogeneous. To cope with this fact the spectral mixture analysis is used for the analysis of the images as it allows the analysis at a sub-pixel level. This method also functions as a data reduction method and offers the advantages of being very fast and easy to use. It might also be implemented in a semi-automated system.

The satellite images, available for this study, cover the whole of the City of Vienna and the surrounding area. Different land cover types are present here, ranging from woodlands to agricultural areas, densely built-up areas to mixed residential areas, water areas to parks. Two different parts of Vienna are selected to demonstrate the proposed methods.

A number of studies, covering the area analysed in 4 and 5, have been undertaken in the recent past. Among these are classifications using neural pattern classifiers (Fischer et al. 1994), and an analysis using classical classification techniques and texture analysis (Steinnocher 1994).

The thesis consists of three main parts. The first part covers the analysis of Landsat TM satellite images of Vienna using spectral mixture analysis. The second part examines how suitable the results of the spectral mixture analysis are to deduct different land use classes from them. The last part shows how the results of the spectral mixture analysis, calculated for two satellite images, can be used to determine where construction activities actually have taken place. This information may then be used to aid the update of the land use data base.

2. Some Fundamental Features of Remote Sensing

Remote sensing is a data collection method, where the sensor is remote from the phenomena; that is, it is not in direct physical contact with them (Colwell (1984, cited acc. Jensen 1986)). Remote sensing thus differs from in situ sensing, where the instruments are immersed in, or physically touch the objects of measurement (Avery and Berlin 1992). Although sensors may be used from different platforms like aircrafts, spacecrafts, or satellites, the term remote sensing will refer in this work only to remote sensing by satellites.

2.1. Electromagnetic Radiation

Remote sensors measure the electromagnetic radiation (EMR) returned by the earth's natural and cultural features that have first received energy from the sun or an artificial source such as a radar transmitter. Because different objects return different types and amounts of EMR, it is the objective of remote sensing to detect these differences and thus make it possible to identify and assess a broad range of surface features and their conditions, e.g. healthy and stressed plants. The entire range of EMR comprises the electromagnetic spectrum. It is divided into nine different spectral regions, which are defined by their wavelengths (Avery and Berlin 1992). Table 1 shows the different spectral regions and their corresponding wavelengths.

Table 1: Spectral Regions with Corresponding Wavelengths

Spectral Region	Wavelength (μm)
Gamma and X rays	< 0.01
Far Ultra Violet	0.01 - 0.2
Middle Ultra Violet	0.2 - 0.3
Near Ultra Violet	0.3 - 0.4
Visible (Blue, Green, Red)	0.4 - 0.7
Near Infrared	0.7 - 1.5
Middle Infrared	1.5 - 5.6
Far Infrared	5.6 - 1,000
Microwave and Radio Waves	> 1,000

Source: Avery and Berlin (1992, p. 6)

The major wavelengths utilised for the sensing of earth resources in the visible and infrared (IR) range are between about 0.4 and 12 μm. The significance of the different spectral ranges lies in the interaction mechanism between the electromagnetic radiation and the materials being interrogated. Each wavelength has its own capacities in terms of the information it can contribute to the remote sensing process (Richards 1986). Figure 1 shows the average spectral-response curves for six materials in the range of 0.4 μm to 0.9 μm.

Figure 1: Average Spectral Response Curves for Six Materials
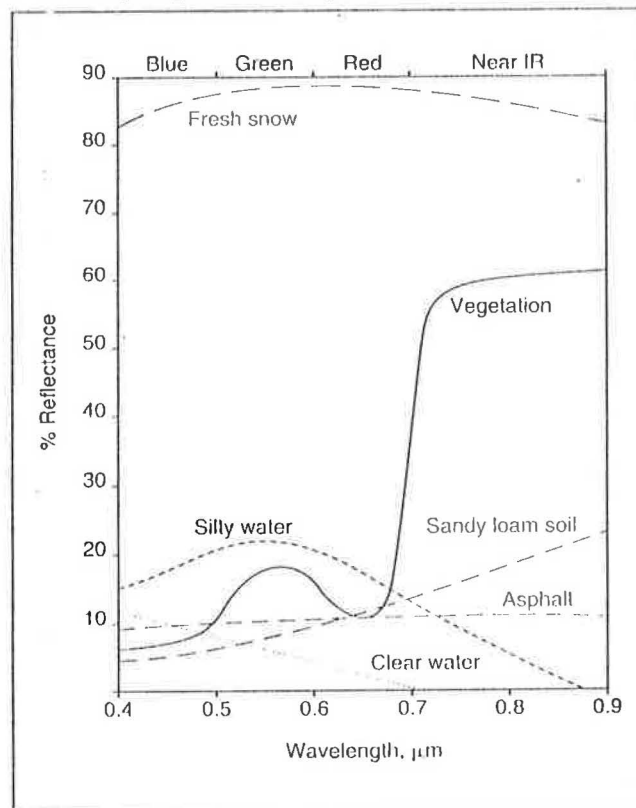
Source: Avery and Berlin (1992, p. 42)

Fresh snow and asphalt have a relatively stable reflectance across the whole range. Vegetation, water, and soil have considerably different reflectance characteristics in the visible (0.4 - 0.7 μm) and IR (> 0.7 μm) regions.

2.2. Spaceborn Scanner Systems

Scanners on satellite systems can be divided in across-track, or whiskbroom scanners and along-track, or pushbroom scanners. Across-track scanners view the ground in a contiguous series of narrow ground strips at right angles to the flight path. The forward motion of the platform causes new ground strips to be covered by successive scan lines (see Figure 2a). The incoming light is directed to spectrum-separation devices (e.g. prisms and dichroic gratings), where it is divided into a number of discrete bands or channels. Along-track scanners represent a new generation and form images without a scanning mirror. This technique uses the forward motion of the platform to sweep a linear array of detectors accross ground scene, with one detector for each ground resolution cell and spectral band (see Figure 2b). The length of the array projected through the optical system defines the swath width, and the size of the individual detectors determines the ground resolution cell (Avery and Berlin 1992).

Figure 2: Track Scanners

(a) Across-Track Scanner **(b) Along-Track Scanner**
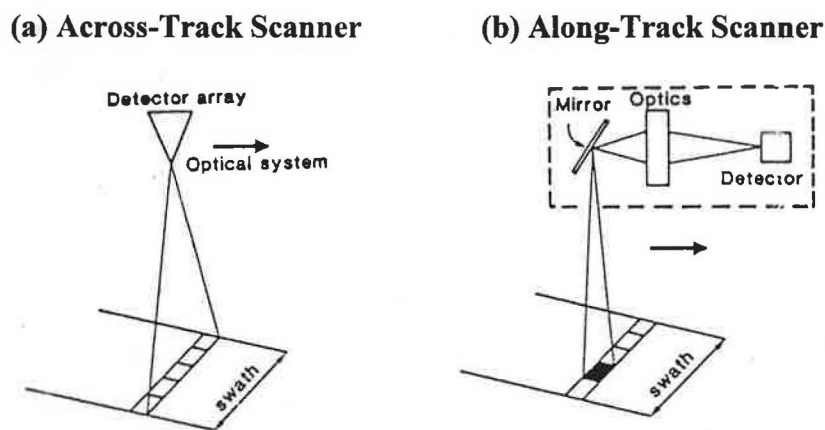
Source: Mather (1988, p. 43)

Detectors convert the radiation reflected from the ground to proportional electrical signals. Analog-digital converters translate them to discrete digital numbers (DNs), from which a digital image can be constructed. To create visible images the numerical data can be transformed into video signals, which enable the images to be seen on a screen, or they can be transferred to a hardcopy. As the information content of a digital image is expressed in

numerical form, analyses and manipulations can be accomplished by mathematical means (Avery and Berlin 1992).

A digital remotely sensed image is typically composed of picture elements (pixels) located at the intersection of each row i and column j in each of the k bands of imagery (see Figure 3). These data should be in perfect geometric registration. The brightness value (BV) at each pixel location is usually represented by a number ranging from 0 to 255 (8-bit scale). This value may be modulated to produce a grey shade ranging from black (BV = 0) to white (BV= 255) (Jensen 1986).

Figure 3: A Digital Remotely Sensed Image with Brightness Value Range and Associated Grey Scale
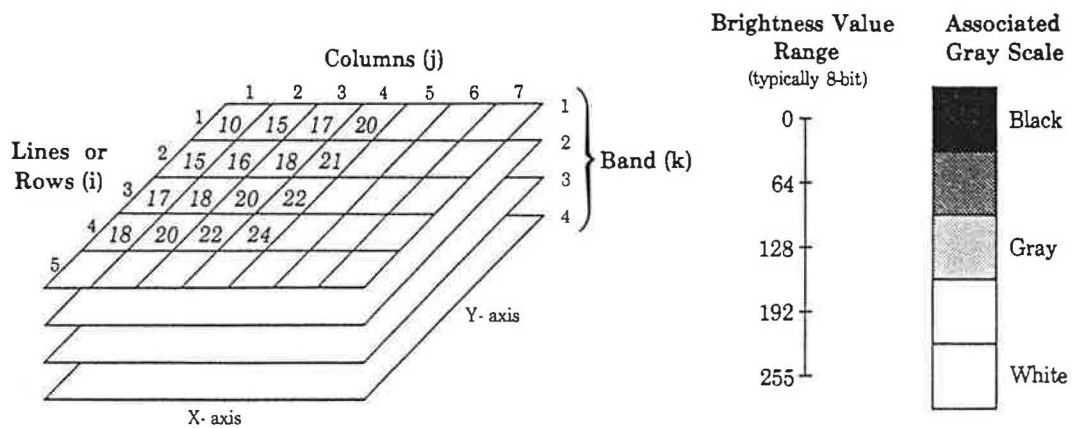
Source: Jensen (1986, p. 12)

Satellite Orbit

Earth observation satellites orbit the earth in either a sun-synchronous or a geostationary orbit. Satellites in a sun-synchronous orbit pass over all places on earth having the same latitude at approximately the same local time. These orbits, at an altitude of approximately 700 to 1,500 km (Richards 1986), are usually used for earth resource satellites as the sun illumination conditions are consistent. Sun elevation, relative position, and intensity still vary with the seasons, but every scene has the illumination of the same time of day. Geostationary satellites maintain a stationary position relative to the earth. They orbit the earth at an altitude of 36,000

km in the same direction as the earth's rotation and are used for weather predictions (Aronoff 1989).

Resolution

When examining the information from remotely sensed imagery four types of resolution must be considered: the spectral, spatial, temporal, and radiometric resolution. The spectral resolution refers to the dimension and number of specific wavelength intervals in the electromagnetic spectrum, to which a sensor is sensitive. The spatial resolution is the dimension of the ground-projected instantaneous-field-of-view. In order to detect a feature, the spatial resolution of the sensor system should be less than half the size of the feature measured in its smallest dimension. The temporal resolution refers to how often a given sensor obtains imagery of a particular area. The radiometric resolution defines the sensitivity of a detector to differences in a signal strength as it records the radiant flux reflected or emitted from the terrain (Jensen 1986, p. 4).

Landsat Thematic Mapper

In the period of 1972 to 1984 five Landsats (for "land satellite") were launched. A thematic mapper (TM) was placed on Landsats 4 and 5 of which the latter is still operating in 1995. The TM is a scanning optical-mechanical sensor system (across-track scanner) that records reflected and emitted energy in the visible, reflective-IR, middle-IR, and thermal-IR regions of the electromagnetic spectrum. It collects data in seven different bands which were chosen according to their value in the discrimination of vegetation type and vigour, plant and soil moisture measurement, distinction of clouds and snow, and identification of hydrothermal alteration in certain rock types. The spatial resolution is 30 x 30 m² for bands 1 - 5 and 7, and 120 x 120 m² for band 6 (see Table 2) (Jensen 1986, p. 30).

The Landsat 5 orbits the earth in a sun-synchronous near-polar orbit (inclination 98.2 °) at an altitude of 705 km, crossing the equator at 9:45 AM, and covers the whole earth in 16 days with 14.5 orbits per day (see Figure 4). The radiometric resolution has a range of 256 digital numbers (8 bits) (Lillesand and Kiefer 1994, p. 463).

Table 2: TM-Bands with Corresponding Wavelength and Resolution

TM-Band	Wavelength (μm)	Resolution (m)
1	0.45 - 0.52 (blue)	30 x 30
2	0.52 - 0.60 (green)	30 x 30
3	0.63 - 0.69 (red)	30 x 30
4	0.76 - 0.90 (reflective-IR)	30 x 30
5	1.55 - 1.75 (mid-IR)	30 x 30
6	10.4 - 12.5 (thermal-IR)	120 x 120
7	2.08 - 2.35 (mid-IR)	30 x 30

Source: Jensen (1986, p. 30)

Figure 4: Sun-Synchronous Orbit of Landsat-5
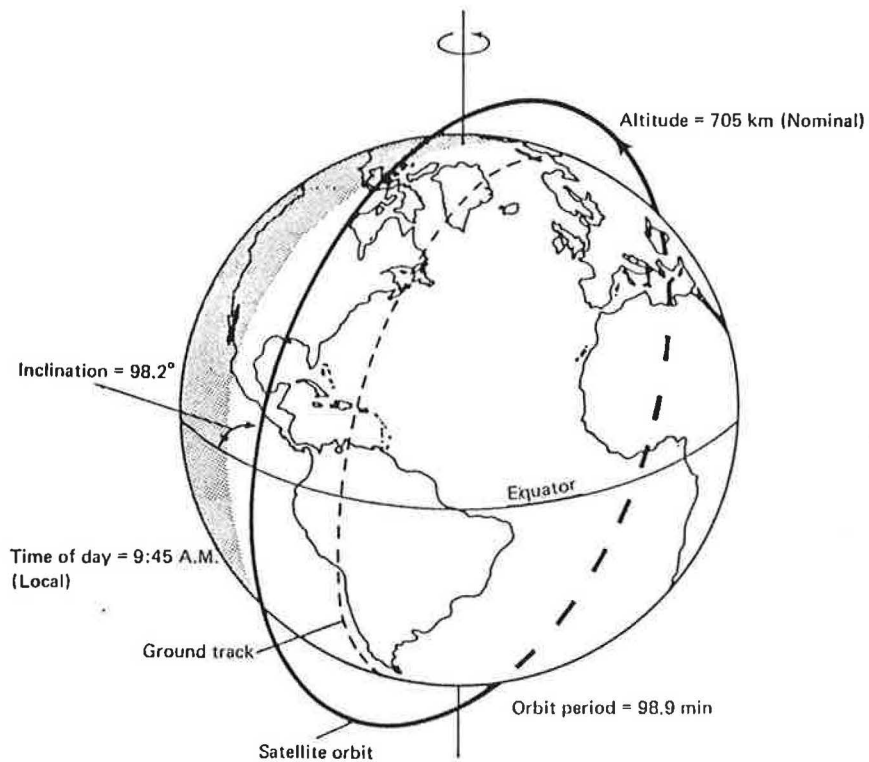
Source: Lillesand and Kiefer (1994, p. 463, adapted from NASA diagram)

Figure 5: Image Formed as Slanted Parallelogram due to Earth Rotation
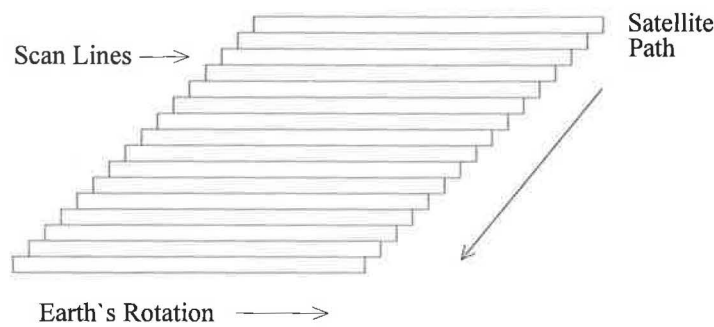
Source: Adapted from Richards (1986, p. 44)

One TM-scene covers a nominal ground area of 185 km across-track by 170 km along-track. Due to the earth rotation the image incorporates rotational skew and is represented as a slanted paralleogram (see Figure 5) (Avery and Berlin 1992).

2.3. Digital Image Processing

Remote sensing images recorded in a digital format express the information content in numerical form. The processing of this information is called digital image processing and encompasses four major areas of computer: preprocessing, enhancement, classification, and dataset merging operation (see Aronoff 1989, p. 405).

Image restoration or preprocessing uses computer routines to correct a degraded digital image to its intended form. It is usually a precursor to the steps that follow. Algorithms have been developed to recognise and remove several types of errors and distracting effects from digital images. They include geometric distortions, noise patterns, variations in solar illumination angle, and atmospheric haze.

Image enhancement improves the detectability of objects or patterns in a digital image for visual interpretation. Enhancement can be divided into the following categories: contrast stretching, spatial filtering, edge enhancement, directional first differencing, multispectral band rationing, simulated natural colour, and linear data transformations.

Image classification uses quantitative decision rules to classify or identify objects or patterns on the basis of their multispectral radiance values (as such, the normal output is analogous to

an image map requiring little or no visual interpretation). This is an information extraction process that involves the application of pattern recognition theory to multispectral images. Image classification analyses the spectral properties of various surface features (e.g. crops) in a multiband image and sorts the spectral data into spectrally similar categories by the use of predefined, numerical decision rules.

Data-set merging involves computer routines to integrate multiple sets of data from the same location so that congruent measurements can be made (representative types of information include geographical, geological, geophysical, geochemical, and multispectral radiance data). It allows for the simultaneous analysis of many types of information for the same ground area taken at different wavelengths, at different times, or by different sensors.

3. Data and Software

3.1. Data

Satellite Data

For the following study two Landsat TM quarter scenes (quadrant I of scene 189/27), observed on June 5, 1986 and July 1, 1991 are used. Of the seven bands the thermal band (band 6) is not utilised as it has a much lower resolution than the other bands (120 x 120 m² compared to 30 x 30 m²). The scenes were geocoded to the Gauß-Krüger co-ordinate system (Buchroithner 1989) and interpolated with the nearest-neighbour method (Jensen 1986). The spectral mixture analysis is carried out for both quarter scenes independently. For the display of the results two areas were selected. The first, examined in chapter 4 and 5, covers the area, for which land use data are available (see below). For the change detection in chapter 6 an area in the Northeast of Vienna was selected.

Land Use Data

The digital land use data database was set up by the City of Vienna in 1986 on the basis of orthophotos. The data are in vector format and each polygon delimits an area of homogeneous land use. For this study land use data, which cover the area of the first selected subscene, was provided by the City of Vienna. Thematically the land use data are divided into 42 classes, 39 of which appear in the selected subscene. In order to compare the vector formatted land use data with the raster formatted satellite data, the land use data were transformed into a raster format with a resolution of 5 x 5 m². This led to a reduction of the number of polygons from 3,822 to 3,540. All the polygons which do not fill out the majority of at least one 5 x 5 m² pixel are lost. As the resolution of the satellite images is 30 x 30 m², these regions would not have been suitable for an analysis so that this loss does not present a problem. The rasterised polygons will from now on be called regions. Table 3 shows the different land use classes and the number of regions for each class that appear in the chosen area.

Table 3: Land Use Classes with Number of Polygons in each Class within the Study Area

Land Use Class	Number of Regions	Land Use Class	Number of Regions
Administration	143	Museums	7
Allotments	65	Outdoor Baths	9
Barracks	2	Parks	162
Broadcasting	0	Port Installations	2
Building Sites	57	Railway	37
Camping Sites	1	Religious Institutions	89
Car Parks	82	Residential Areas	1,606
Cemeteries	7	Residential Areas with Garden	317
Commerce and Trade	291	Sand and Gravel Production	0
Common Utilities	39	Schools	139
Day Care Centres	36	Sport Fields	50
Drainage	27	Theatres	13
Energy Supply	10	Traffic Facilities	28
Exhibition Grounds	2	Trams	23
Fields	19	Unproductive Land	25
Forest	20	Vineyards	43
Gardening	12	Water Areas	31
Gymnasiums	4	Water Treatment	1
Hospitals	21	Water Supply	4
Industrial Plants	31	Yards	13
Lawn	72	Zoos	0

Figure 6 shows the landaus map of the area analysed in chapter 4 and 5. Each polygon defines an area of homogeneous use. At the bottom of figure 6 is the centre of the City of Vienna, the Danube goes from the North to the East, and in the middle a mixed residential area with vineyards in the North. This part of Vienna covers everything from built-up areas to farming

Figure 6: Land Use Map of Area under Investigation

0   400   1000m
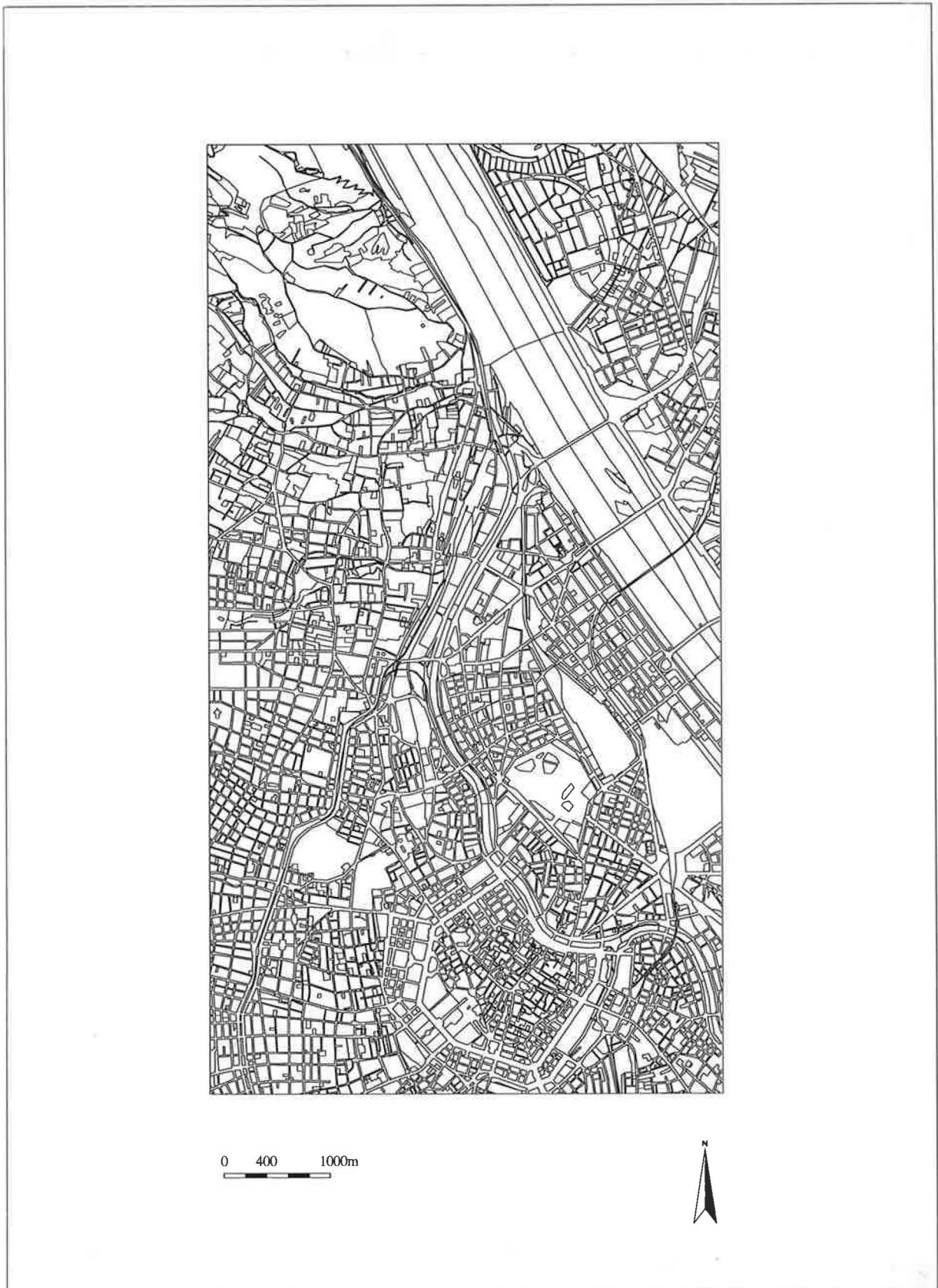
areas, from water-bodies to mixed residential areas and is therefore very suitable to test the method used for the analysis of the satellite image.

3.2. Software

For the geocoding of the satellite images the computer package ERDAS 6.02 of Erdas. Inc., was used. The spectral mixture analysis which will be described in 4. has been carried out using the public domain program "Image Processing Workbench" (IPW) (Frew 1990). It was also used to carry out the principal component analysis as a first step of analysing the satellite image. For converting of the land use data into a raster format, the classification as described in 5., the change detection as outlined in chapter 6, and for the production of the maps, ARC/INFO 7.0 of ESRI, Inc. has been used.

4. Spectral Mixture Analysis

A number of methods exist for classifying satellite images. They can be divided in supervised and unsupervised classification procedures. In a supervised mode some of the land cover types are known beforehand, and the analyst attempts to locate specific sites in the image that represent homogeneous examples of these known land cover types. These are the training sites, because the spectral characteristics are used to "train" the classification algorithm by calculating multivariate statistical parameters for each training site. According to these parameters the rest of the image is classified. In an unsupervised classification the data are clustered into different spectral classes according to statistically determined criteria. The clusters are then labelled by the analyst (Jensen 1986). These methods have the disadvantage of assigning a certain class to each pixel. This problem is most apparent if the area in question is very heterogeneous. This is especially the case in an urban environment, and to overcome this problem the strategy proposed in this study is to modify the classical approach by a transformation. The information gained by the transformation is then used to apply the classical procedure (see chapter 5) and the change detection procedure (see chapter 6).

The multispectral or vector character of most remote sensing data allows the generation of new sets of image components or bands by applying transformations. The components represent an alternative description of the data. A vector space with as many dimensions as there are bands may be constructed. In the case of the Landsat TM with six bands (excluding the thermal band) this leads to six dimensions. Examples for different types of transformations are principal components transformation and band arithmetics (Richards 1986). These techniques are used for the enhancement of images as well as prior to classifications.

The principal component analysis uses the covariance matrix to calculate a set of new, transformed variables called principal components. These are largely independent of one another. Geometrically, the components represent a set of mutual orthogonal and independent axes that are fitted to the original data. The first new axis contains the highest percentage of total variance in the data, decreasing with each succeeding axis (Avery and Berlin 1992).

Band arithmetics are simple transformations, and use addition, subtraction, multiplication, and division of the pixel brightness values from two bands of image data to form a new image. Ratios of different spectral bands from the same image are useful for reducing external effects such as seasonal changes in sunlight illumination angle and intensity (Richards 1986).

The above mentioned techniques have a very limited ability of extracting information. Except for the vegetation index, which gives very reliable information due to the reflectance characteristics of plants (see Figure 1), the results of the techniques mentioned above have to be interpreted after the transformation. They may also vary considerably from image to image. To overcome this restriction the transformation technique used here is the spectral mixture analysis. It allows the user to determine the thematic information contained in each transformation component.

The spectral mixture analysis has been used in a number of studies in the natural environment, as for instance for the estimation of sediment concentration in the Amazon River (Mertes et al. 1993), the analysis of rock and soil types at the Viking Lander 1 Site (Adams et al. 1986), the abundance of vegetation in deserts (Smith et al. 1990), the analysis of inland tropical water (Novo and Shimabukuro 1994). The only study using spectral mixture analysis in an urban environment deals with the analysis of data collected by an airborne thematic mapper (ATM) of the University College of Swansea, UK (Foody and Cox 1994).

4.1. Method

The spectral mixture analysis tries to estimate how each ground pixel's area is divided up among different cover types. This is known as mixture modelling, and the aim is not a single map of symbols (the classification image) but a series of images, each the size of the original image, and each giving the proportion of a different land cover type. The data resulting from this analysis is of a quantitative and qualitative nature (Settle and Drake 1993). The lower the spatial resolution and the higher the heterogeneity of the area in question, the more different land cover components are encompassed in one pixel. The objective is to determine the proportion of each of the land cover components present in each pixel.

To calculate these proportions a set of spectra is defined called "image endmembers", representing the land cover types in question. When mixed using the appropriate rule, these endmembers reproduce all of the pixel spectra. The endmembers are selected from areas which show only or nearly only the land cover in question, and which receive maximum illumination. In addition, an endmember called "shade" is introduced, which accounts for variations in lighting at all scales (e.g. changes in incidence angles, shadows cast by topographic features, subpixel shadows cast by trees, and so forth). The endmembers are defined from pixels which must be as pure as possible. The shade endmember can be derived from a pixel in a shadow cast by a topographic feature (Adams et al. 1989).

The maximum number of endmembers corresponds to the number of spectral bands of the satellite image. Due to the fact that some bands are highly correlated the number of endmembers is in general smaller than the number of bands. To identify the intrinsic dimensionality of the data, the principal component analysis may be used. The number of components showing meaningful information is the relevant number of endmembers (Settle and Drake 1993).

Once the endmembers are defined the fractions of each endmember in each pixel may be calculated by applying the appropriate mixing rule. The general equation for mixing is (Adams, et al. 1989):

$$DN_c = \sum_{n=1}^{N} F_n \cdot DN_{n,c} + E_c \tag{1}$$

where

$$\sum_{n=1}^{N} F_n = 1 \tag{2}$$

with

DN_c radiance in channel c,

N number of endmembers ,

F_n fraction of endmember n,

$DN_{n,c}$ radiance of endmember n in channel c,

E_c error for channel c of the fit of N spectral endmembers.

Equation (1) converts the DN value of each pixel in each channel to the equivalent fraction (F_c) of each endmember as defined by the endmembers ($DN_{n,c}$). The error (E_c) accounts for that part of the DN-value which is not described by the mixing rule. The equation (2) introduces the constraint that all fractions of one pixel must sum to one.

As long as the number of endmembers is smaller than the number of bands an overdetermined set of equations exists which may be solved using the linear-least-square method by minimizing the residual vector v (Kraus 1990):

$$b + v = A\,x \tag{3}$$

with

A   design matrix of the endmember matrix A(m,n) and rank r, where m is the number of bands and n the number of endmembers,

b   vector of observations (m,1),

x   vector of unknowns (n,1),

v   residual vector (m,1), to be minimized.

From this follows v = A x - b. The residual vector v is minimized to calculate the unknowns x (Kraus 1990):

$$v^T v = Min = (A\,x - b)^T (A\,x - b) = x^T A^T A\,x - 2\,b^T A\,x + b^T b \tag{4}$$

$$\frac{dv^T v}{dx} = d(v^T v) = 2\,x^T A^T A - 2\,b^T A = 0 \tag{5}$$

From this follows that vector x satisfies:

$$A^T(b - A\,x) = 0 \tag{6}$$

i.e. the residual vector v = b - A x is orthogonal to the columns of A (Björck 1967). If $m \geq n$ and $r = n$ then x satisfies (Golub (1965 cited acc. Linnik 1961)):

$$A^T A x = A^T b. \tag{7}$$

From this follows that the fraction vector x may be calculated by:

$$x = (A^T A)^{-1} A^T b. \tag{8}$$

The fractions of each endmember in each pixel (x) are calculated by multiplying the coefficients matrix (calculated by multiplying $(A^T A)^{-1} A^T$) with the DN-vector of the pixel in question (b).

A modified Gram-Schmidt regression is used to invert the endmember matrix and determine the coefficients with which the fractions are calculated (Frew 1990). Two different variants of the Gram-Schmidt regression exist to solve this orthonormal basis (OB) problem, which is defined as the problem to find an orthonormal basis for span $\{a_i.. ,.., a_n\}$, when independent vectors $a_i.. ,.., a_n \in \Re$ are given (Golub and Loan 1989). Two vectors (x, y ≠ 0) are orthogonal if the scalar product is zero ($x^T y = 0$). Orthonormal vectors are defined as orthogonal vectors, which are normalised vectors with a length of one. A vector x is normalised by the multiplication with the scalar $\|x\|^{-1}$ (Hackl and Katzenbeisser 1992).

The classical Gram-Schmidt (CGS) method calculates the orthogonal vectors one at a time, and the modified Gram-Schmidt (MGS) procedure progressively adjusts all the linearly independent vectors (Farebrother 1974). The MGS is very suitable for solving the OB problem if orthonormality is critical and the vectors to be orthogonalised are fairly independent (Golub and Loan 1989).

Once the coefficients have been determined, the fractions for each endmember are calculated by:

$$F_n = \sum_{c=1}^{C} DN_c \cdot coeff(n, c) \tag{9}$$

with

F_n fraction of endmember n,

C   number of channels,

DN_c radiance in channel c,

coeff(c,n) coefficient of endmember n in channel c.

(9) is carried out for every pixel and every endmember. The shadow fraction is calculated by subtracting the sum of all fractions of the pixel in question from one. The results are stored in fraction images, one for each endmember, including one for the shadow endmember and one for the rms error (see below).

Testing the Results of the Spectral Mixture Analysis

Three ways exist to evaluate the results of the spectral mixture analysis. These are the visual analysis, the calculation of the root-mean-squared (rms) error and the calculation of the fraction overflow (Adams et al. 1989).

With the visual analysis of the fraction images, the analyst determines whether they are consistent with other information existing about the area in question, e.g. do the high fractions in vegetation appear where they ought to appear. If the patterns do not correspond with the additional information obtained by ground truthing or other sources then the model constructed may not be correct.

The second test is the calculation of the rms error. The rms error is based on the E_c term of equation 1, squared and summed over all M image channels (see (10)) (Adams et al. 1989)

$$\varepsilon = \left[c^{-1} \sum_{c=1}^{k} E_c^{\,2} \right]^{1/2} \tag{10}$$

with

ε root-mean-squared (rms) error

k   number of Channels

The rms error is calculated for every pixel individually and can also be visualized as an image. It may also be calculated for the whole image, showing the overall rms error. A small rms error is an indication of a mathematically good model. A large rms error indicates that the model has not been constructed correctly.

The third test is the computation of the fraction overflow. Reason dictates that the fractions of the land cover components must lie between zero and one, but if the model in not constructed correctly fractions may fall outside this range. As the endmembers are supposed to represent 100 % of the land cover in question, any pixel having a higher portion of the land cover as compared to the endmember pixel, will have a fraction higher than one. To satisfy the constraint that all the fractions of a pixel must sum to one, another fraction of this pixel will be below zero.

If the model is not satisfactory according to the tests described above, the endmembers must either be changed, deleted, or additional endmembers defined. The following rules aid in the selection of new endmembers. An overflow in a fraction image is an indication for a pixel, which represents the land cover better then the pixel used for the definition of this endmember up to now. An overflow and a high rms error in a pixel may be due to an unmodelled endmember represented by that pixel.

4.2. Application of Spectral Mixture Analysis

Endmember Selection

As pointed out in 4.1. the number of principal components analysis gives an indication of the intrinsic dimensionality of the satellite image and thus of the number of endmembers necessary to analyse the image. The result of the principal component analysis, i.e. the

variance explained by each component, conducted for the 1986 image using the correlation matrix, is shown in Table 4.

Table 4: Variance Explained by Principal Component Analysis

Principal Component	Variance Explained in %	Cumulated Variance in %
1	59.62	59.62
2	34.74	94.36
3	4.22	98.59
4	0.94	99.527
5	0.38	99.90
6	0.10	100.00

The first three principal components explain over 98 % of the total variance of the image data. Because of this the intrinsic dimensionality of the data may be assumed to be three, and thus the number of endmembers limited to three. The endmembers selected for the analysis represent vegetation, water and built-up areas. An additional endmember for shade is defined to account for the variations in lighting due to changes in incidence angle and variations that are caused by shadows (Adams et al. 1989) in the image. To define the endmembers, pixel vectors are examined which only or nearly only represent the land cover in question. The pixel vector for vegetation has a very high value in the near infrared band 4, as this band is best for picking up vegetation. The pixel is located in an area covered by forest in the North of Vienna.The endmember for water is defined by a pixel vector located in a faster flowing part of the Danube in the North of Vienna, and the endmember for built-up areas is defined by a pixel vector located in an administration building. Figure 8 shows band 4 of the subscene of the satellite image with the locations of the three endmembers.

As shadow represents areas not or badly illuminated, the endmember was defined as zero in all six bands although it is possible that the shade endmember is greater than zero, owing to instrumentation offsets and/or gain, skylight scattering, and so forth (Adams and Smith 1986). Figure 7 shows the spectral plot of the endmembers for vegetation, built-up areas and water.

Figure 7: Spectral Plot of the Endmembers for Vegetation, Building, and Water
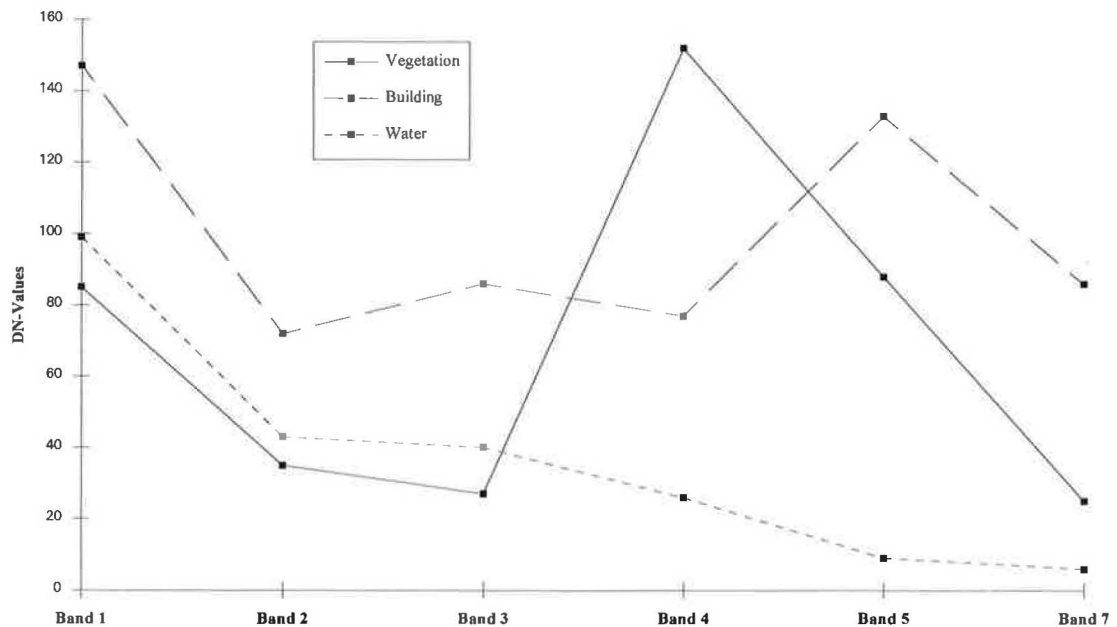
Fraction Images

The fraction images are calculated according to the procedure described in 4.2. for each endmember, including the shadow endmember. In addition the rms image is calculated, giving the rms error for each pixel.

For the visualization of the fraction images, they are rescaled according to the rules in Table 5, and the rms error-image is rescaled according to Table 6. Lighter colours in the fraction images indicate a higher fraction of the respective endmember. Lighter shades in the rms error-image indicate a higher error.

Table 5: Rescaling of Fraction Images

Fraction	Fraction Image Value
< -1	0
-1 to 0	0 to 100
0 to 1	100 to 200
1 to 1.55	200 to 255
> 1.55	255

Table 6: Rescaling of Rms Error-Image

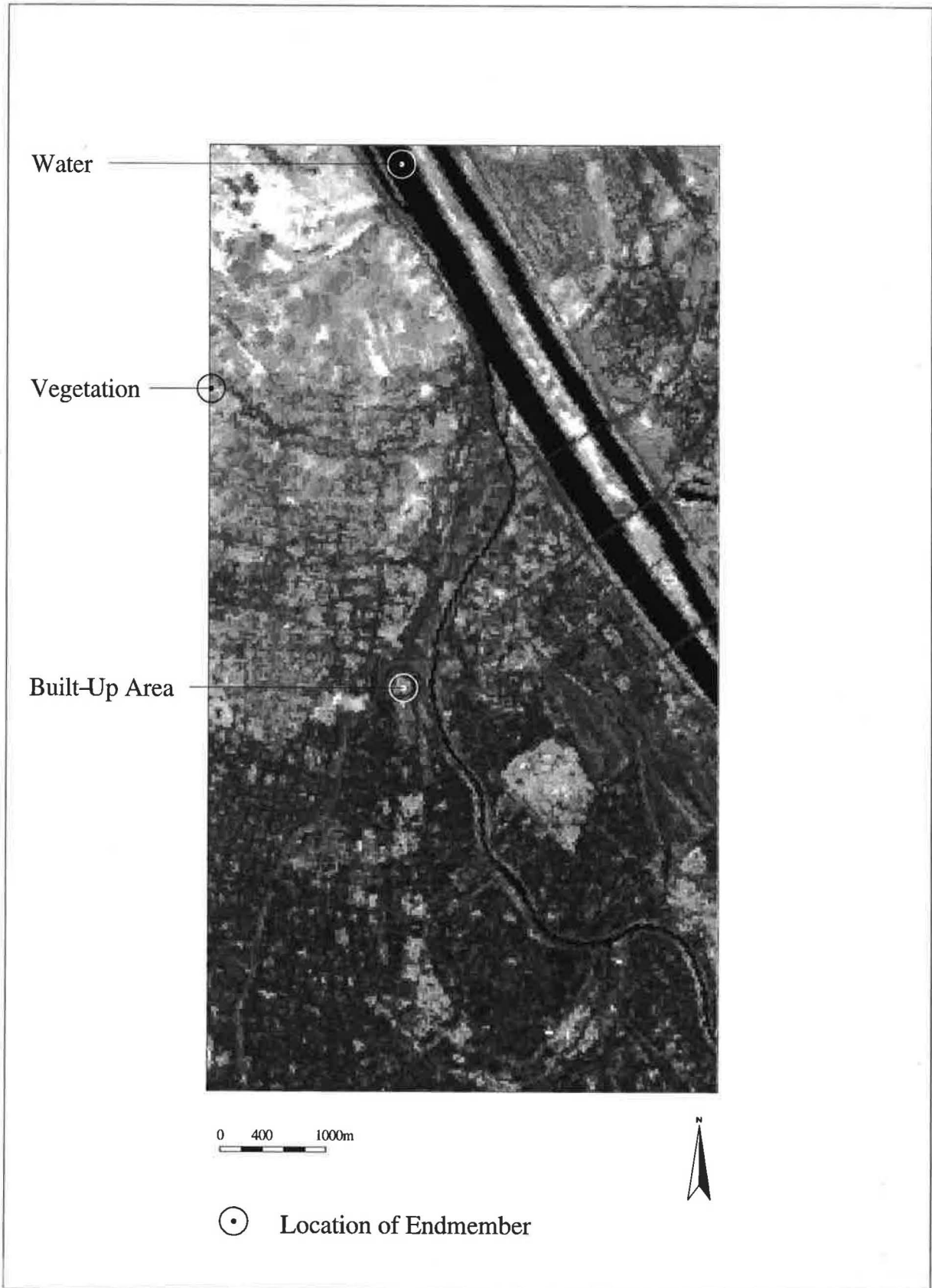| Rms error	Rms error-image value
0 to 15	0 to 255
> 15	255

The highest values in the fraction image for vegetation (Figure 9) are in the north-western part of the image, an area covered mostly by forest. The values decrease until they reach their minimum in densely built-up areas and water regions. In the centre of the city the parks are very distinct from the surrounding buildings. The fraction image for built-up areas (Figure 10) shows as light areas the very heavily built-up areas like the city centre, train stations, and hospitals. In the water regions and forest areas the values have their minimum. Vineyards appear in very light colours and may be confused with heavily built-up areas when looking at this fraction image alone. This fact is put in perspective when examining the water fraction image (Figure 11). The Danube can be made out very clearly, values are low in built-up areas and even lower in areas with vegetation. The lowest values are found in areas with vineyards, and thus make it possible to differentiate between vineyards and built-up areas by looking at the fraction images for buildings and water simultaneously.

The rms image (Figure 12) shows a very even distribution of the error across the whole image with the exception of a few small spots. These spots are either due to instrumental errors, or to areas which reflect in a very untypical fashion for this image. In quantitative terms the average error for every pixel is 3.4 DN-values.

Another way of displaying the data is to create a colour composite of the fraction images. This makes it possible to view all fraction images simultaneously, and to examine how the different areas are influenced by the fraction images. Figure 13 shows the colour composite with red being used for the fraction image for built-up areas, green for vegetation, and blue for water. The land use data has been laid over the colour composite. Residential and built-up areas can be easily distinguished from areas covered by plants or water. The parks (green) in the city centre are clearly visible, and the vineyards (yellow) in the North are very distinct from built-up areas, which show as bright red.

Figure 8: Band 4 with Locations of Endmembers

Figure 9: Fraction Image for Vegetation

No Vegetation   Vegetation

0   400   1000m
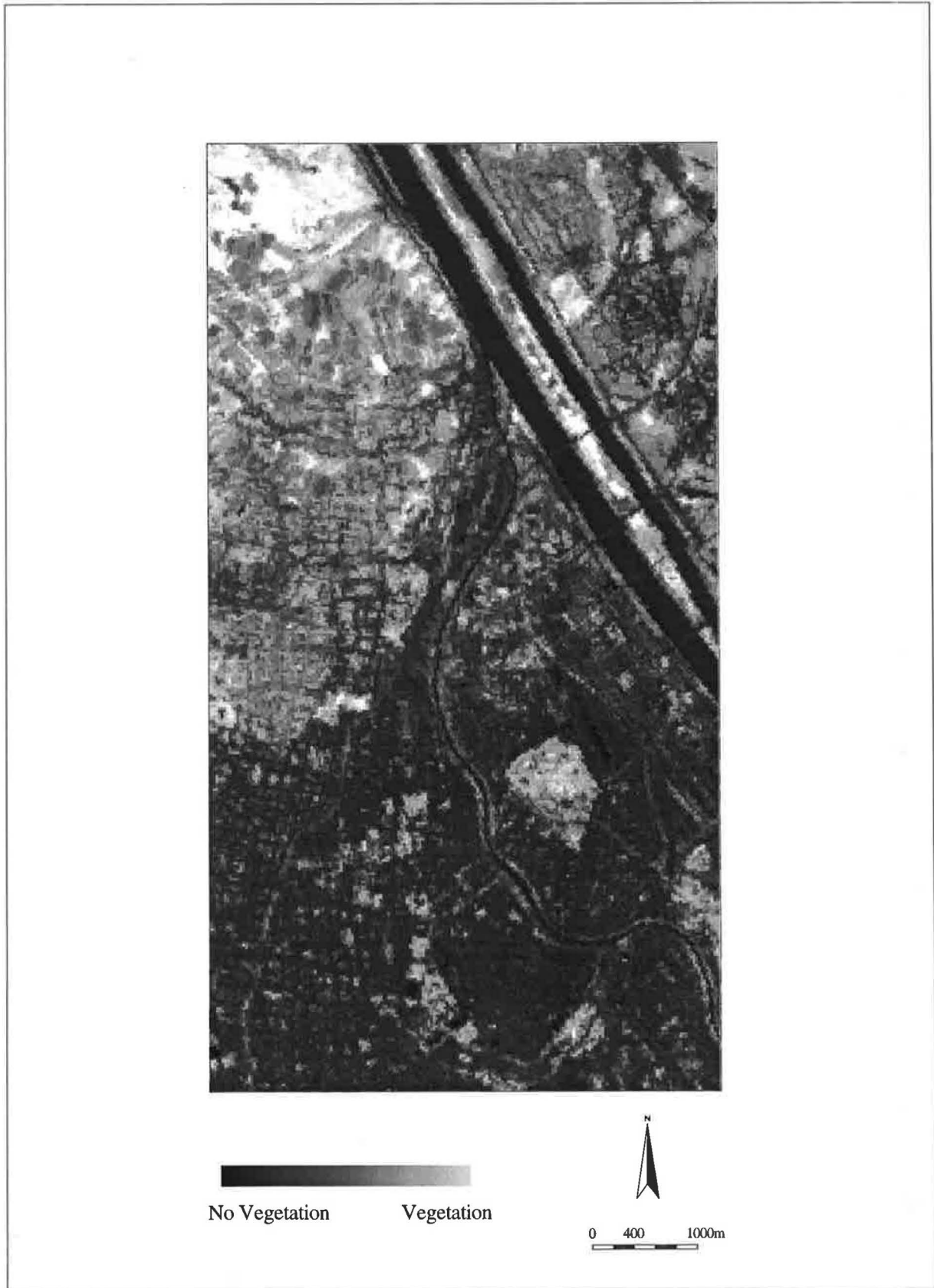
Figure 10: Fraction Image for Built-Up Areas

No Buildings   Built-Up

0   400   1000m
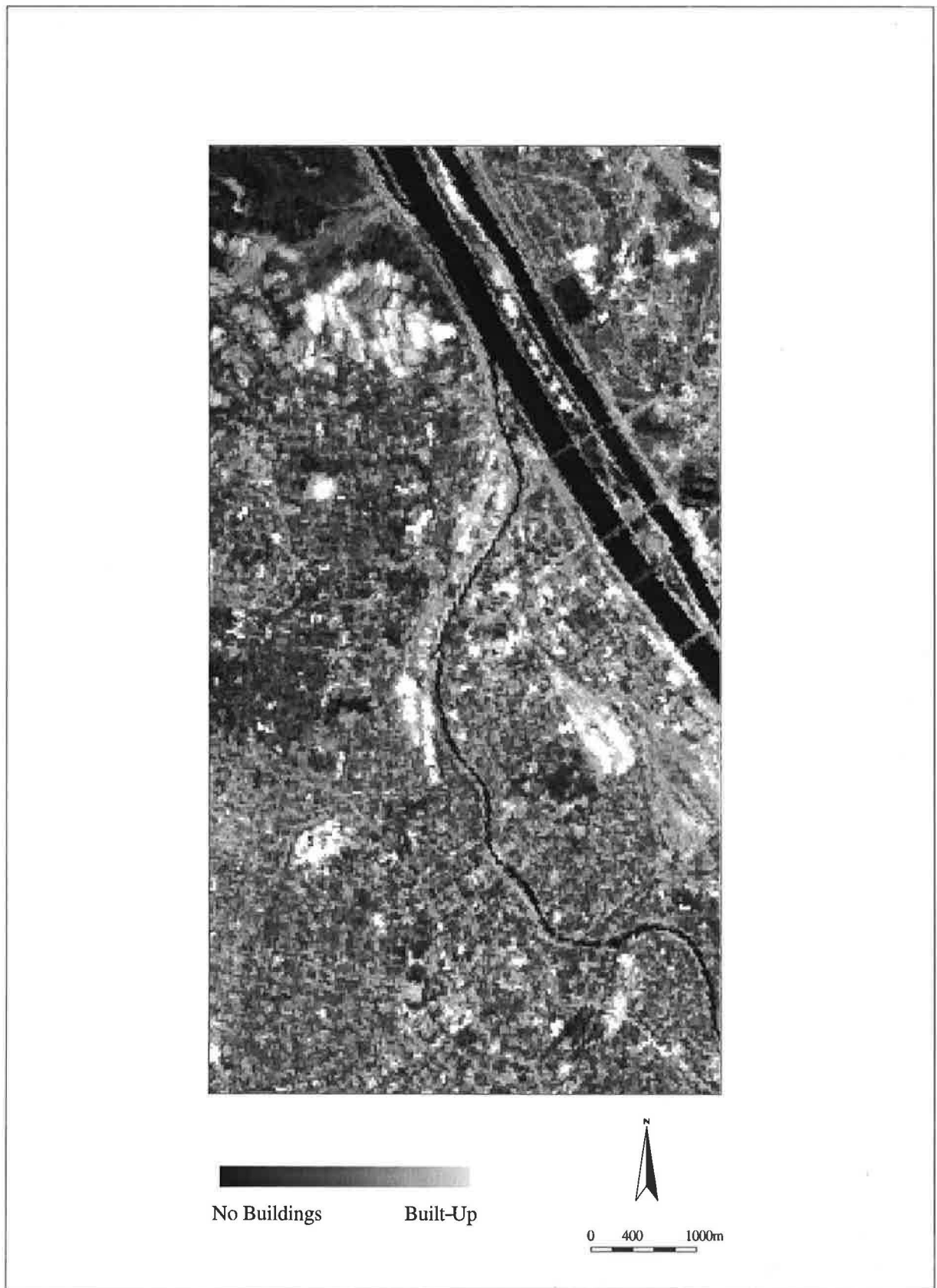
Figure 11: Fraction Image for Water

No Water   Water

N

0   400   1000m
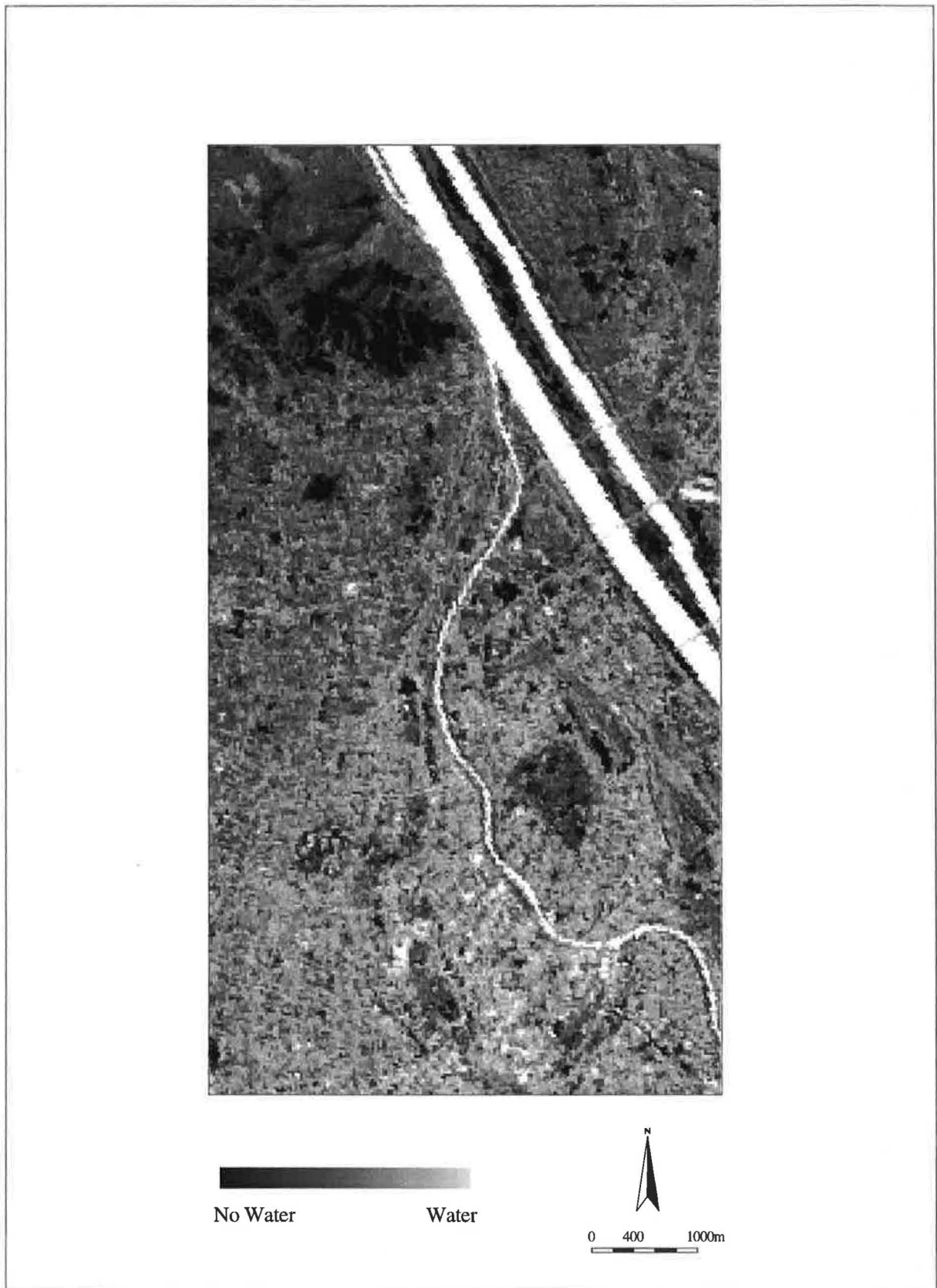
Figure 12: Rms Error-Image

Low Rms Error   High Rms Error

N

0   400   1000m
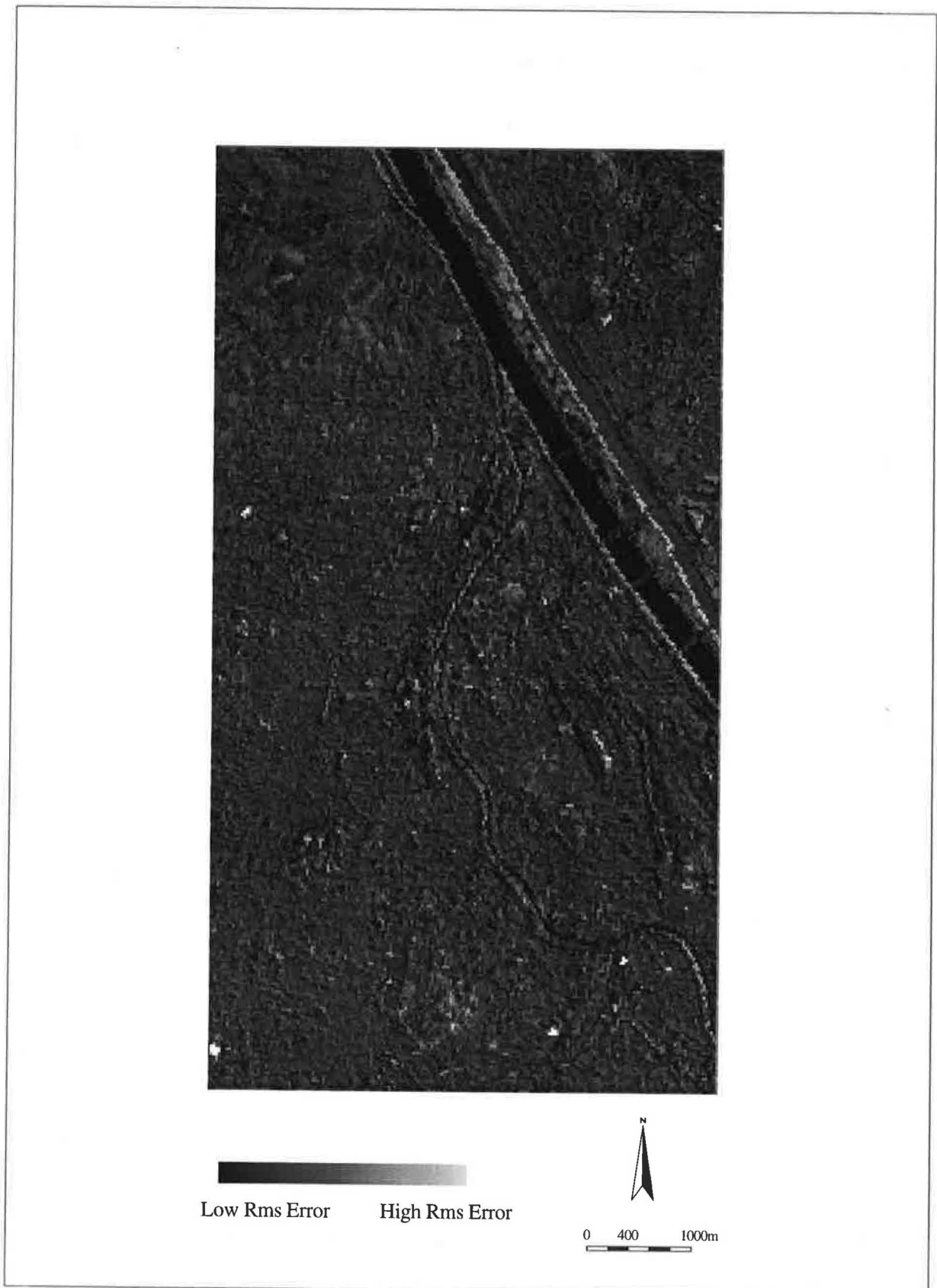
Figure 13: Colour Composite of Fraction Images

Building Vegetation Water

N

0   400   1000m
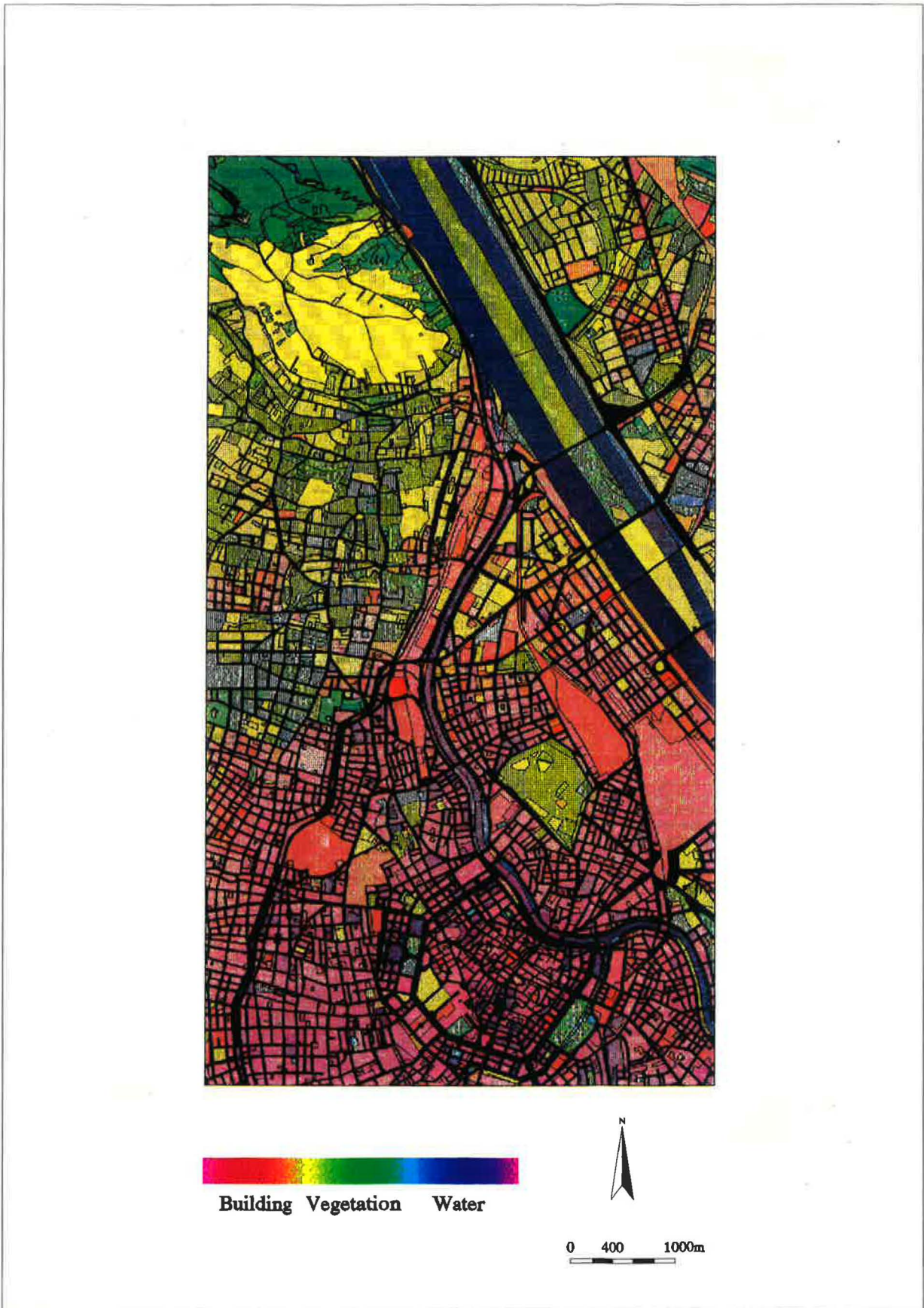
The next step of the analysis is to integrate the results of the SMA with the land use data, to determine how suitable the fraction images are to actually deduct different land use classes from them. So far only a transformation of the satellite image according to the information provided by the endmembers has been done.

5. Integration of Land Use Data with Fraction Images

The purpose of this section is to examine how suitable fraction images are to derive different land use classes from them. The fraction images themselves are not classifications, but give the proportions of vegetation, buildings, and water in the area covered by the satellite image. The procedure for the comparison and the subsequent classification can be seen in Figure 14. To make a comparison between the vector based land use data and the raster based fraction images possible, the land use data were transformed into a raster format with a resolution of 5 x 5 m². Because of this transformation, the number of polygons was reduced from 3822 to 3540. The reduction of the number of polygons is due to those polygons which do not have the highest portion in at least one 5 x 5 m² pixel. Considering the resolution of the satellite image of 900 m², these regions are not suitable for the analysis because of their small size. The rasterized polygons will from now on be called regions. The next steps are to assign a land use class to each region (as defined in 3.1) on the basis of the fraction images and the evaluation of the results of this classification.

5.1. Classification of Regions

The land use data has 42 different classes, and 39 of these are represented in the study area. When examining these classes (Table 3), it is apparent that many classes differ only in their functional but not in their spectral properties, e.g. a building block may house a school, a hospital, apartments, and so forth. To make a comparison between the land use data and the fraction images possible, nine main classes were selected from the 39 land use classes (forest, residential area with garden, residential area, field, park, water area, vineyard, lawn, and rail). All remaining classes may be attributed to one or more of these main classes, which will be taken into account when the results of the classification are evaluated.

The aim of the classification is to assign every region to one of the nine main classes. Figure 14 shows the steps of the classification of the regions. After the transformation of the land use data into a raster format, the resulting raster image is laid over each of the fraction images (Figure 14 top). The means for every region in each fraction image are calculated using (11).

$$m_{r,f} = p^{-1} \sum_{n=1}^{p_r} d_{n,r,f}$$ (11)

with

$m_{r,f}$ mean of region r in fraction image f,

p_r number of pixels in region r,

$d_{n,r,f}$ fraction value of the nth pixel d in region r and fraction image f.

The mean for a region within one fraction image is calculated by summing the fraction values of all pixels lying within that region, and dividing the sum by the number of pixels. This procedure is carried out for each fraction image, and results in one vector v_r for every region containing one mean value for every fraction image (Figure 14).

To obtain the reference data according to which the regions are classified, the mean values for each main class are aggregated for each fraction image. Of these aggregated values the mean is calculated producing again a vector, only this time for the nine main classes for each fraction image:

$$a_h = c_h^{-1} \sum_{n=1}^{c_h} v_n \qquad \text{for all h}$$ (12)

with

a_h aggregated vector for each main class h,

c_h number of regions per main class,

v vector of mean values of a region belonging to main class h,

h number of main classes.

Figure 14: Transformation of Vector into Raster Format and Calculation of the Mean for each Region

Land use data in vector format

Transformation into raster format

Land use data in raster format

Overlay with fraction image

Fraction image overlay

Calculate mean of proportion d for all pixels within region r

Mean $m_{r,f}$ of region r in fraction image f

⎯⎯ Border of region r as defined by land use data

▱ Pixel at location x,y within one region as defined by the land use data

▨ Pixel at location x, y in region r containing proportion d of landcover within fraction image f

The results are the mean proportions of each main class in every fraction image. In the last step all regions are assigned to the one of the h main classes to which the mean values (m_r) of the region r under examination have the smallest distance (($m_r - a_h)^2$ is a minimum).

5.2. Results of Integration

The result is a classification of the whole study area with each region related to one of the main classes (Figure 15). Colours are assigned to all nine main classes are assigned according to the results of the classification. Dark green stands for forest, very light green for light vegetation, magenta for residential area, orange for residential area with garden, grey for field, light green for park, red for heavily built-up area (defined by railway in the main classes), blue for water, and yellow for vineyards. As is to be expected, the residential areas lie mainly in the central area of the city. Going further north there are less heavily built-up residential areas, but mainly residential areas with garden although here often classified as parks. This is not so surprising considering the features of a park and a residential area with garden. Both have some vegetation and some buildings thus making a differentiation very difficult. The north-western and northern areas are covered by forests and vineyards.
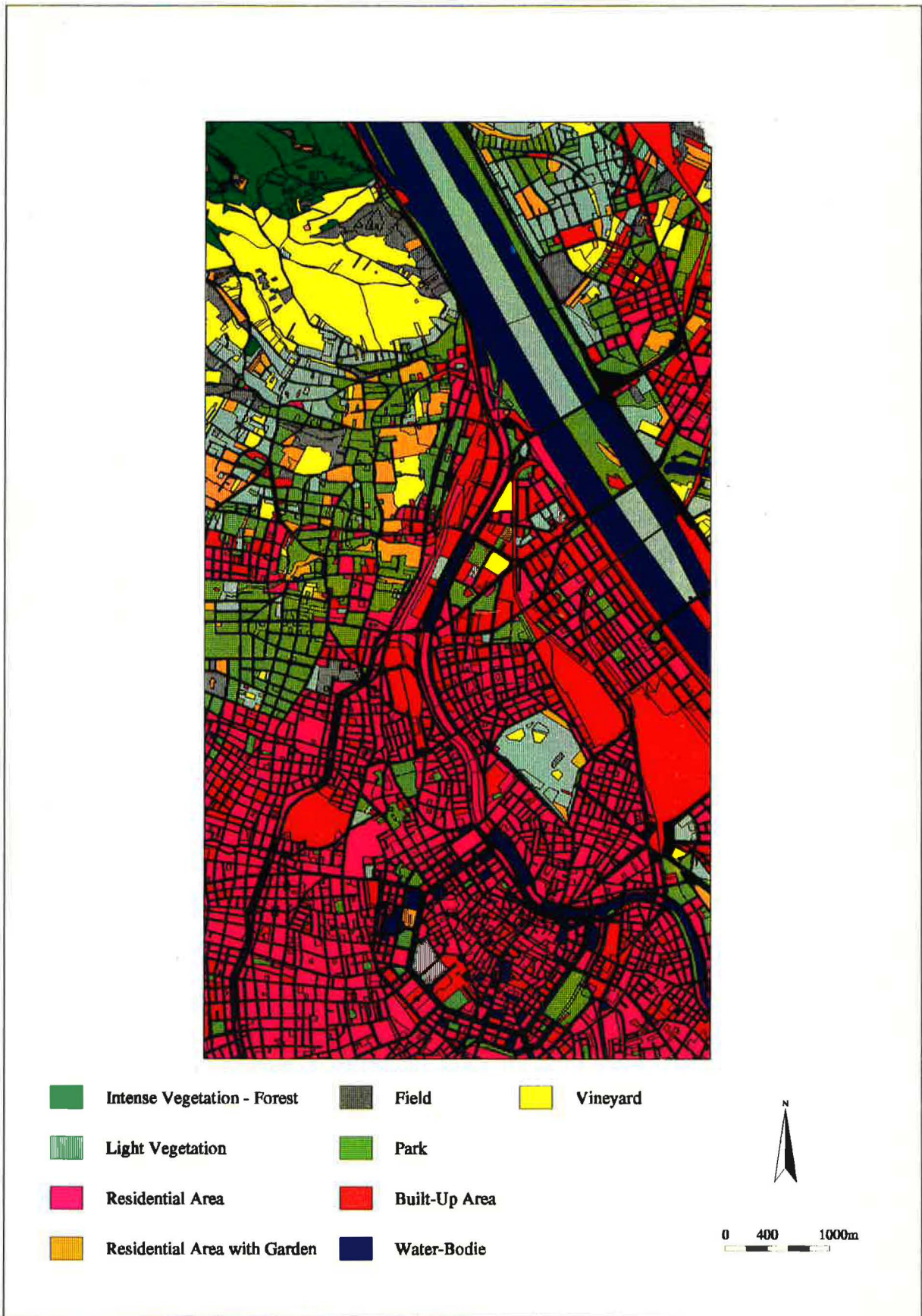
The next step is to compare the results of the classification with the land use data in order to determine how well the classification, and thus how suitable the method is to derive land use data. As the land use data has 39 classes which appear in the study area, rules have to be established to determine the accuracy of the classification. These rules are shown in Table 7.

These rules take into account that the different functional properties may not always be distinguished satisfactorily by spectral data and also that one class may be a member of more than one main class. The results of the evaluation of the classification can be seen in Figure 16.

The land use data has been superimposed to the evaluation image so that each polygon depicts one region. The regions which are classified correctly are coloured green, and those which are not classified correctly are coloured red. Some of the red coloured regions can be explained very easily, as for example the ones in the area of the Donaukanal. This canal is fairly narrow and low, compared to the surrounding area, lined on all sides by concrete, and therefore water is very difficult to distinguish. The greatest difficulty lies in the upper part of the image, where many regions are classified as residential areas with garden although, according to the

## Figure 15: Results of Classification of Regions

Intense Vegetation - Forest   Field   Vineyard

Light Vegetation   Park

Residential Area   Built-Up Area

Residential Area with Garden   Water-Bodie

N

0   400   1000m

Table 7: Rules for Determining the Accuracy of the Classification

Main Class / Land Use Class	Forest	Residential Area with Garden	Residential Area	Field	Park	Water Area	Vineyard	Lawn	Rail
Administration			X						X
Allotments		X		X	X			X	
Barracks			X						X
Building Sites		X	X	X	X		X	X	X
Camping Sites		X	X	X	X		X	X	X
Car Parks		X	X	X	X		X	X	X
Cemeteries	X	X		X	X		X	X	
Commerce and Trade			X						X
Common Utilities		X	X		X				X
Day Care Centres		X	X		X				X
Drainage		X	X	X	X		X	X	X
Energy Supply			X						X
Exhibition Grounds			X						X
Fields	X			X	X		X	X	
Forest	X			X					
Gardening	X	X		X	X		X	X	
Gymnasiums			X						X
Hospitals		X	X		X				X
Industrial Plants			X						X
Lawn		X		X	X		X		
Museums			X						X
Outdoor Baths		X	X	X	X		X	X	X
Parks		X		X	X			X	
Port Installations			X						X
Railway			X						X
Religious Institutions		X	X		X				X
Residential Areas			X						X
Residential Areas with Garden		X		X	X			X	
Schools		X	X		X				X
Sport Fields		X	X	X	X		X	X	X
Theatres			X						X
Traffic Facilities			X						X
Trams			X						X
Unproductive Land		X	X	X	X		X	X	
Vineyards				X			X		
Water Areas						X			
Water Treatment			X						X
Water Supply			X						X
Yards		X	X	X	X		X	X	X

X: Land use class and main class are considered similar, and thus the classification correct.

Figure 16: Evaluation of Classification

Correctly Classified

Misclassified

0   400   1000m
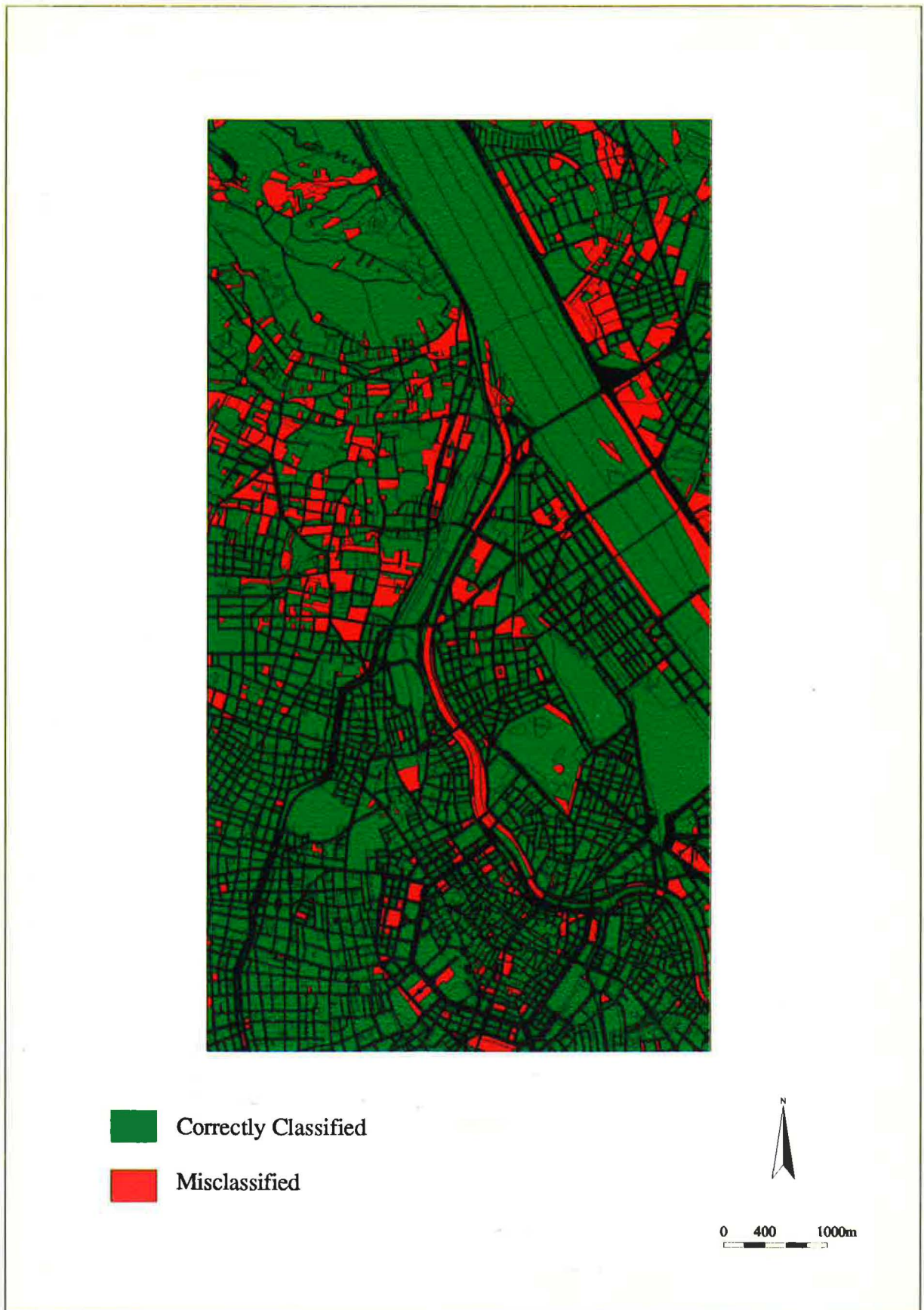
land use data, these regions should be densely built-up residential areas. This is easily explained, as the land use data classifies those regions, which have residential buildings and some green areas, which do not belong to a single household but to the whole building, as normal residential areas. The problem here lies not within the classification but within the definition of residential areas in the land use database.

When examining the quantitative analysis of the classification accuracy (Table 8), one can see that 84% of the regions are considered to be accurate and 16% of the regions are evaluated as not accurate. When looking at the area, the results are even better. 88% of the area are classified correctly and 12% are considered to be different.

Table 8: Quantitative Analysis of the Classification Accuracy

Classification	Number of Regions	Regions in %	Area in ha	Area in %
Correct	2,959	84	3,757	88
Not Correct	581	16	518	12
Total	3,540	100	4,275	100

The results presented here show a high classification accuracy and allow the assumption that the fractions represent the area under investigation very well. Therefore in the next chapter an attempt is made to use fraction images for a change detection.

6. Change Detection

6.1. Conventional Methods

Monitoring changes in the environment is a problem faced by different institutions today. Especially government agencies have the task to detect and record changes. The challenge is to gather the necessary information at acceptable costs in the intervals required, and to develop suitable techniques for detecting changes. For urban studies this task is typically done by photo interpretation. Small-scale photographs (e.g. 1:10,000 and larger) and vertical stereopairs from mapping cameras are used for urban studies on a general scale. Air photography has the disadvantage of being very expensive in obtaining the pictures, making regular repeat coverages prohibitively expensive. Analogue photographs also take a long time and a lot of manpower to be analysed (Richards 1992). Compared to these methods satellites offer, despite their still rather coarse resolution (Landsat TM, 30 x 30 m^2) an number of advantages. These are necessary for a system, if it is to be used for change detection and are (Jensen 1986):

- Regular repeat coverage,
- Record data from the same geographic area at the same time of day,
- Maintain the same scale and look-angle,
- Record reflected radiant flux in consistent and useful spectral region,
- Inexpensive compared to other methods as for instance aerial photography.

As the spatial resolution of satellite systems improves, the easier it will be to take advantage of these features, but even today satellite images may be used for change detection purposes. The applications are limited of course. In urban areas it is usually not possible to distinguish individual buildings, but it may be determined whether and where changes have taken place. The aim of this study is to show how fraction images of satellite images, recorded at different dates, can be used to determine where building activities have take place.

To get a successful change detection it is necessary to chose a time of year when one may expect, that the land cover types in question show large differences in their spectral response. It is also advisable to have images which are take at approximately the same time of year and ideally with comparable weather conditions. Before it is possible to perform change detection it is necessary to geocode the images.

A number of procedures exist for change detection: (see Jensen 1986, pp 37):

- Image Differencing
- Image Overlay
- Image Ratioing
- Classification Comparison
- Principal Component Analysis
- Change Vector Analysis

For **image differencing**, two bands from images recorded at different times are subtracted from one another. For images recorded with values ranging from 0 to 255 (8-bit) the potential range for the result is from -255 to 255. Pixels where changes have occurred should have either very low or very high values. Pixels with no changes should be around zero. The problem is where to put the cut-off value for change/no change. This might either be done by calculating the standard deviation from the mean or it might be done interactively, where the user tries different values and decides, based on his knowledge about the area, where the cut-off value should be. The changes, which are detected must be interpreted as to the type of change, as the bands contain no qualitative and limited quantitative information.

A method comparable to image differencing is image overlay, where two or three bands are laid over one another using different colours. Colour changes in different areas show where changes might have taken place and if the changes were positive or negative ones. Again the problem is interpreting the changes, as there is no qualitative information.

Ratioing is a technique where a band from one date is divided by a band from another date. Ratio transformations tend to remain invariant to changes in viewing conditions (e.g. sun

angle, and so forth) and thus improve the accuracy of the change detection compared to image differencing. Pixels, where no changes have take place will have a value around one, areas, where changes have take place will have values either higher or lower one.

Classification comparison identifies change by comparing two independently produced classification maps. The accuracy of this method depends on the initial classifications. Especially the heterogeneity of urban areas produces many mixed pixels, which lower the accuracy of the individual classification maps. As a result of this, too much change may be identified (Toll et al. (1980, cited acc. Jensen 1986))

For **principal component analysis** a set of mutually orthogonal variables is calculated. Each consecutive variable accounts for the maximum amount of variability within the original data. The principal components calculated for images taken at different dates may aid the identification of areas, where changes have taken place. Either the principal components are calculated separately for each image and then compared, or the images are combined and the components calculated. The thematic contents of each principal component may not be influenced and may change from image to image.

With **change vector analysis**, the spectral characteristics of an area before and after a change are examined. If both spectral characteristics are plotted on the same graphic a change vector may be determined. This vector describes the direction and the magnitude of the change. A threshold is set up to decide whether a change has taken place or not.

The methods described above have the disadvantage of either supplying no information as to the nature of the change or being very cumbersome to implement. The following section will show how fractions images may be used to determine changes over time.

6.2. Change Detection using Fraction Images

Two Landsat TM images were available for this study. The images were recorded on June 5, 1986 and July 1, 1991. The time of year, when the images were recorded, is therefore approximately the same, and although it is a time of year, when a lot of changes take place in

the vegetation, they are still close enough to allow a successful comparison. For the change detection a different area was chosen, as the area examined in chapter 4 and 5 is already heavily built up with very few changes taking place. The new area is a development area and thus very well suited for the demonstration of this method.

The method used to detect urban growth is closely related to image differencing. The main use of image differencing so far was in subtracting bands or principal components from one another. Both have the disadvantage that neither individual bands nor principal components contain information which may be regularly related to a special land cover type. There is neither a qualitative or a quantitative element present. Fraction images on the other hand offer the advantage of containing a priori defined qualitative information (certain land-cover type) and quantitative information (values within the fraction images are between 0 and 100%) The method to detect changes suggested here is to subtract fraction images, which represent the same land cover type, calculated from satellite images recorded at different dates. If the fraction images represent the same type of information changes should be clearly seen, as the fraction images values must be higher or lower for pixels, where the land cover type has changed compared to a pixel from an earlier date. Two premises must be satisfied before a change detection may be attempted. First it is necessary to make sure that the fraction images represent the same information. To check this the histograms of the fraction images are compared. If the information is the same, then the general shape of the curve must be approximately the same, except for minor differences, which are due to the land use changes and seasonal changes. Also one must make sure that the information shown by the fraction images is as pure as possible i.e. only the land cover type in question is represented. If that is not the case, the change detection will be negatively influenced, and methods must be found, to remove these influences. To do that the inclusion of one or more other fraction images in the change detection might be advisable.

The spectral mixture analysis was carried out for both images. The rules for determining the endmembers laid down for the first fraction image were used to define the endmembers in the second image, which allows the analysis to be done very quickly. The results are two fractions for every endmember, one for each date of recording. As the aim is to detect where building

activities have taken place, in a first run only the fraction images for built up areas are examined.

To determine, whether the two fraction images actually represent the same land cover component, the histograms are compared (Figure 17).

Figure 17: Histogram of the Fraction Images for Built-Up Areas for 1986 and 1991
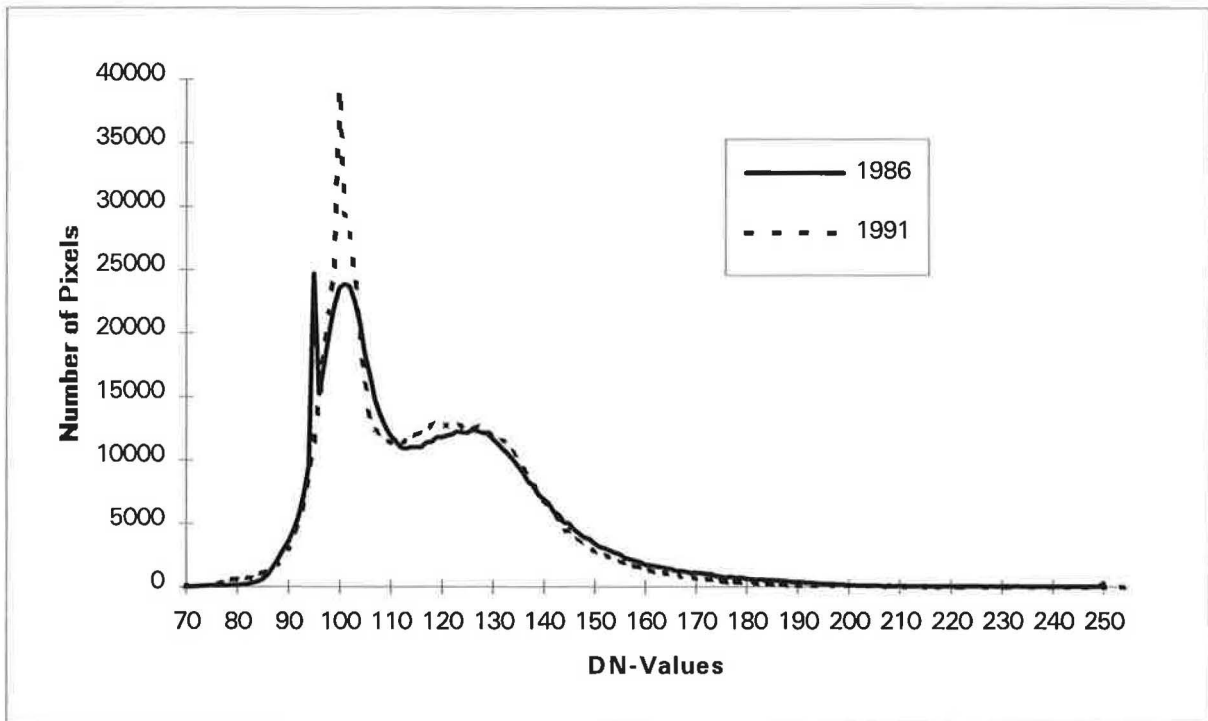
As the histograms of 1986 has a shift of 5 DN-values to right, compared to the histogram of 1991, the 1986 histogram was corrected by these 5 DN-values for the comparison. The histograms have a very similar shape, with the exceptions for a peak at DN-value 95 in the 1986 histogram and a peak at DN-value 100 in the 1991 histogram. These peaks are due to different cloud covers in different parts of the image and changes in vegetation. As these differences are in areas, where there are no buildings (a DN-value of 100 is equivalent to a fraction of 0), these slight differences will not affect the change detection.

The next step is the subtraction of the fraction image for 1986 from the fraction image for 1991. The result is a new image, and to show the areas of interest all pixel, which have a positive difference of more than 20, are highlighted. The threshold value of 20 was found to

Figure 18: Result of Change Detection

Likely Changes

Unlikely Changes due to low Water Fraction Image

Water

0   600   1500m
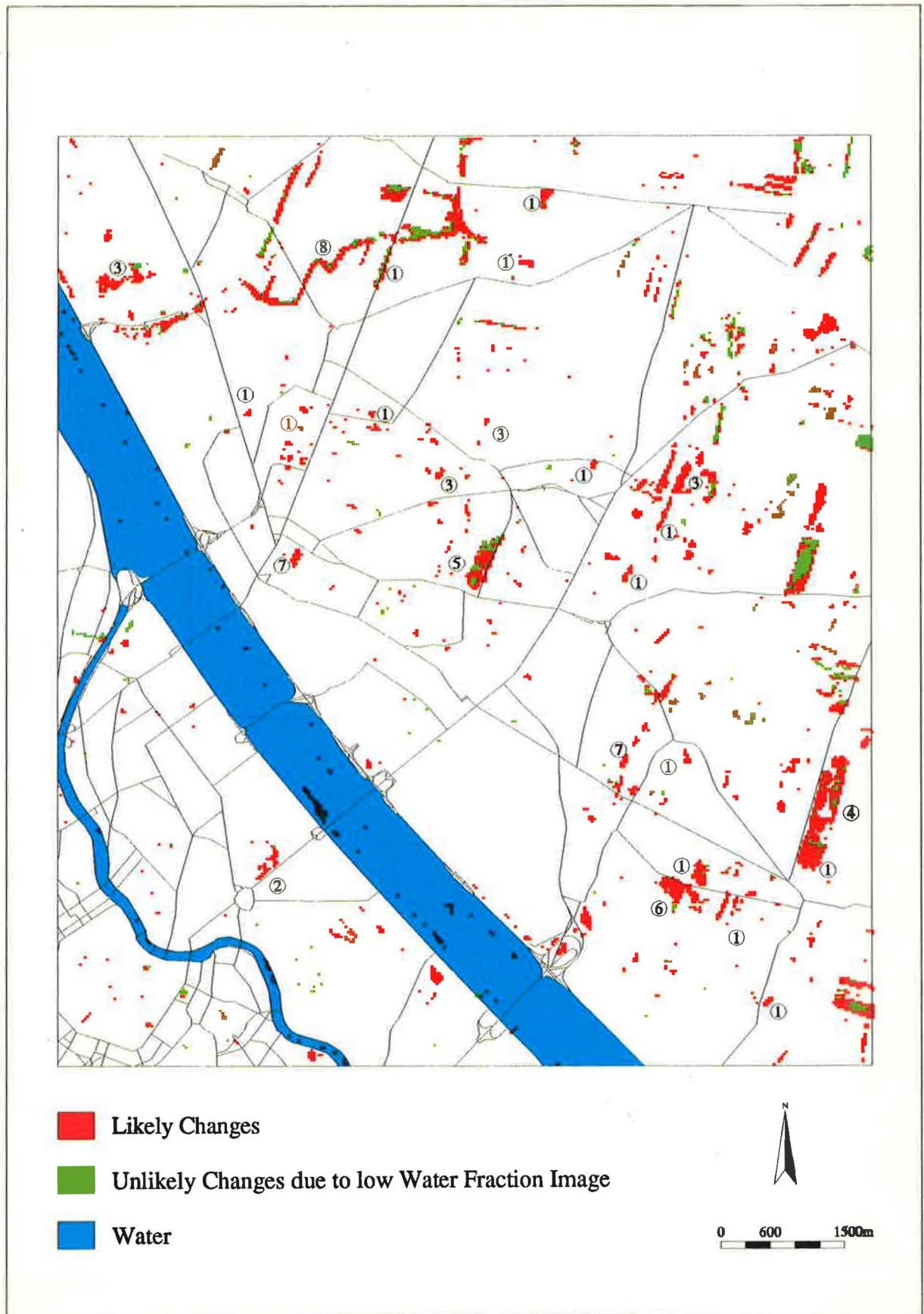
be most suitable after examining different values. A problem encountered here is the differentiation between bare fields and built up areas, as there is a considerable signature overlap (Jensen 1986). To overcome this problem, the fraction image for water from 1991 is also included to make the differentiation more reliable. As pointed out in 4.4.2. the fraction image for water may be used to differentiate between visible soil and built-up areas. The result is a map (Figure 18) which shows where, according to the analysis, changes have taken place (red) or might have taken place, but are more likely to be fields (green). A ground truthing was conducted and the confirmed changes are marked with numbers in figure 18. Table 9 shows to which changes the numbers correspond.

Table 9: Detected Construction Activities from 1986 to 1991

Number in Figure 18	Construction Activity
1	Residential Area
2	Office Blocks
3	Industrial Zones
4	Allotments
5	Veterinarian Faculty (under construction)
6	Hospital (SMZ-Ost)
7	Administration
8	Irrigation Canal (under construction)

23 changes were identified. As may be expected, most changes take place in residential areas (13) and industrial zones (4).

7. Conclusions and Outlook

Satellite images offer a wealth of information which may help us understand and investigate developments in our environment. The challenge is to find suitable techniques to analyse the satellite data and extract the relevant information. The study presented here attempts in a first step to deduct different land use classes and changes over time from satellite images of an urban environment. As such images are very heterogeneous a spectral mixture analysis was applied. This makes it possible to determine the portions of different land cover types within each pixel. The resulting fraction images are then used to determine different land use classes from them. A comparison with an existing land use data base shows a very high accuracy, confirming the suitability of the spectral mixture analysis for this kind of environment.

In the next step the spectral mixture analysis was applied to a second satellite image of the same area, recorded at a different date. The results of the transformations of both images were used for a change detection and to determine those areas, where construction activities have taken place. The result were verified by a ground truthing, confirming most calculated changes.

The procedure presented here for change detection offers a powerful tool for city planers, as it not only gives accurate information as to where changes have taken place but can also be carried out in a very short time. Costs can not only be saved in the collection of the data but also in the analysis of satellite images. If all the land use data of Vienna is available it is possible to determine in which polygons changes have taken place and either simply change the attribute of the polygon or change the polygon itself, if that should be necessary. By combining the benefits of the high spectral resolution of the Landsat TM and the high spatial resolution of newer systems (e.g. panchromatic MOMS) the interpretation of the results could be greatly improved. Here it would be possible to examine those areas, where changes are supposed to have taken place, by a visual analysis of the high resolution data.

The procedure may also be used for other change detection purpose either in an urban or a natural environment. If the data is calibrated then it might also be possible to determine exactly the magnitude of the change.

References

Adams, J. B. and Smith, M. O. (1986): Spectral Mixture Modeling: A New Analysis of Rock and Soil Types at the Viking Lander 1 Site, **Journal of Geophysical Research**, Vol. 91 (No. B8), pp 8098 - 8112.

Adams, J. B., Milton, O. S. and Gillespie, A. R. (1989): Simple Models for Complex Natural Surfaces: A Stretgy for the Hyperspectral Era of Remote Sensing, **Proceedings of IGARSS'89**, Vol. 1, pp 16 - 21.

Aronoff, S. (1989): **Geographic Information Systems**, WDL Publications, Ottawa.

Avery, T. E. and Berlin, G. L. (1992): **Fundamentals of Remote Sensing and Airphoto Interpretation**, Macmillan Publishing Company, New York.

Björck, A. (1967): Solving Linear Least Squares problems by Gram-Schmidt Orthogonalization, **BIT**, Vol. 7, pp 1 - 21.

Buchroithner, M. F. (1989): **Fernerkundungskartographie mit Satellitenaufnahmen**, Franz Deuticke, Wien.

Colwell, R. N. (1984): From Photographic Interpretation to Remote Sensing, **Photgrammetric Engineering and Remote Sensing**, Vol. 50, pp. 1305 - 1307.

Fischer, M. M., Gopal, S., Staufer P. and Steinnnocher, K. (1995): Evaluation of Neural Pattern Classifiers for a Remote Sensing Application, WSG-Discussion Paper 47, Department of Economic Geography, University for Economics and Business Administration, Vienna.

Frew, J. E. (1990): The Image Processing Workbench, Ph. D. Thesis, Department of Geography, University of California, Santa Barbara.

Farebrother, R. W. (1974): Gram-Schmidt Regression, **Applied Statistics**, Vol. 23, pp 470 - 476.

Foody. G. M. and Cox, D. P. (1994): Sub-Pixel Land Cover Composition Estimation using a Linear Mixture Model and Fuzzy Membership Functions, **International Journal of Remote Sensing**, Vol. 15 (No. 3), pp 619 - 631.

Golub, G. (1965): Numerical Methods for Solving Linear Least Squares Problems, **Numerische Mathematik**, Vol. 7, pp 206 - 216.

Golub, G. H., and van Loan, C. F. (1989), **Matrix Computations**, North Oxford Academic, Oxford.

Hackl, P., and Katzenbeisser, W. (1992): **Mathematik für Sozial- und Wirtschaftswissenschaften**, R. Oldenburg Verlag, München und Wien.

Jensen, J. R. (1986): **Digital Image Processing**, Prentice-Hall, New Jersey.

Kraus, K. (1990): **Fernerkundung**, Band 2, Ferd. Dümmlers Verlag, Bonn.

Lillesand, T. M. and Kiefer, R. W. (1994): **Remote Sensing and Image Interpretation**, New York, John Wiley & Sons, Inc.

Linnik, Y. (1961): **Method of Least Squares and Principles of the Theory of Observations**, Traslated from Russion by R. C. Elandt, Pergamon Press, New York.

Mather, P. M. (1988): **Computer Porcessing of Remotely-Sensed Images**, John Wiley & Sons, Chichester.

Mertes, L. A. K., Smith, M. O., and Adams, J. B. (1993): Estimating Suspended Sediment Concentration in Surface Waters of the Amazone River Wetlands from Landsat Images, **Remote Sensing of the Environment**, Vol. 43, pp 281 - 301.

Novo, E. M. and Shimabukuro, Y. E. (1994): Spectral Mixture Analysis of Inland Tropical Waters, **International Journal of Remote Sensing**, Vol. 15 (No. 6), pp 1351 - 1356

Richards, J. A. (1986): **Remote Sensing Digital Image Analysis**, Springer Verlag, Berlin.

Settle, J. J., and Drake, N. A. (1993): Linear Mixing and the Estimation of Ground Cover Proportions, **International Journal of Remote Sensing**, Vol. 14 (No. 6), pp 1159 - 1177.

Smith, O. S., Ustin, L. S., Adams, J. B. and Gillespie, A. R. (1990): Vegetation in Deserts: I. A Regional Measure of Abundance from Multispectral Images, **Remote Sensing of the Environment**, Vol 31, pp 1 - 26.

Steinnocher, K. (1994): **Methodische Erweiterung der Landnutzungsklassifikation und Implementierung auf einem Transputernetzwerk**, Geowissenschaftliche Mitteilungen, Vol. 40, Technische Universität, Wien.

Taranik, J. V. (1978): Characteristics of the Landsat Multispectral Data System, **U.S. Dept. of the Interior**, Open File Report, Sioux Falls, S.D, pp 78 - 187.

Toll, D. L., Royal, J. A. and Davis, J. B. (1980): Urban Area Update Procedures Using Landsat Data, **Technical Papers**, Annual Meeting of the American Society of Photogrammetry.

Curriculum Vitae

Born:	23rd November, 1967, Mödling
1974 - 1978	Elementary School, Maria Enzersdorf Südstadt
1978 to 1981	Grammar-School, Vienna
1981 - 1983	German School, London, England
1983 - 1988	Commercial College, Mödling
1988 - 1996	University of Economics and Business Administration, Vienna
1993 - 1994	University of California, Santa Barbara
1994 - 1995	Scholarship of the Austrian Research Center, Seibersdorf

Publications

Kressler, F. and Steinnocher, K. (1995): Einsatz der Fernerkundung zur Überprüfung der Realnutzung im Raum Wien mittels Spectral Mixture Analysis, **Salzburger Geographische Materialien**, Vol. 22, pp 213 - 222.

Kressler, F. (1996): Change Detection in urbanen Räumen, **Vermessung & Geoinformation**, Vol. 84, No. 1, pp 48 - 51.

Kressler, F. and Steinnocher, K. (1996): Change Detection in Urban Areas using Satellite Images and Spectral Mixture Analysis, XVIII ISPRS Congress, Publication forthcoming.